JOURNAL OF COMPUTATIONAL PHYSICS 9, 75–98 (1972)

Numerical Simulation of Plasmas with Periodic Smoothing in Phase Space

J. DENAVIT*

Plasma Physics Division, Naval Research Laboratory, Washington, D.C. 20390

Received April 20, 1971

This paper presents a "hybrid" method of numerical simulation of collisionless plasmas in which weighted particles are advanced as in particle simulations, but in which the distribution function is reconstructed periodically by a local averaging operation as in numerical solutions of the Vlasov equation. The rates of diffusion resulting from repeated averaging of the distribution function are estimated. These rates indicate that it is possible to minimize the effects of both beaming instabilities and diffusion by properly choosing the frequency of reconstruction of the distribution function. A computer code was written to implement this method and numerical solutions of two-stream instability problems are presented.

1. INTRODUCTION

Computational studies of the dynamic behavior of plasmas have generally been carried out either by using particle simulation methods or by solving the Vlasov equation numerically. The purpose of this paper is to present "hybrid" solutions in which weighted particles are advanced as in particle simulations, but in which the distribution function is reconstructed periodically as in Vlasov solutions by a local averaging operation in phase space. The problems considered are one-dimensional with periodic boundary conditions, and involve only electrons moving over a uniform, positively charged background.

In particle simulation of plasmas, the positions and velocities of a large number of particles moving in their self-consistent (and any externally imposed) fields are computed as a function of time [1–5]. Thus the complete dynamical state of the system is known at every time step, and average quantities of interest, such as number densities or temperatures, are computed whenever desired. The initial positions and velocities of the particles may be chosen either randomly or in ordered manner to simulate the actual initial conditions of the plasma. In a random

* Permanent address: Northwestern University, Evanston, Ill. 60201.

initialization, the initial positions of the particles are chosen to represent the initial density and their initial velocities are chosen at random with probabilities corresponding to the initial velocity distribution. This initialization procedure is simple and conceptually close to actual physical conditions. However, since the number of simulation particles is necessarily much smaller than the number of particles found in actual plasmas, the fluctuations appearing in the averaged quantities, such as the electric field, mean velocity or thermal velocity, are much larger in the simulation plasma than in the actual plasma. These fluctuations may be reduced by increasing the number of simulation particles, but they drop only as $N^{-1/2}$, where N is the number of simulation particles. The number N is, of course, limited by the computer capacity.

When all the simulation particles representing a given specie are identical, many particles are needed to represent the larger values of the distribution function while proportionally few particles are available to represent the smaller values. The discrete nature of the simulation plasma is therefore particularly evident in regions of the phase plane where the density in phase is small, such as in regions corresponding to the tails of the distribution function. Particle simulation methods using weighted particles, all having the same charge over mass ratio, but with varying charges and masses, have been used to improve the representation of the plasma in regions of low density in phase [5]. These methods are useful to study resonant interactions between waves and a relatively small number of particles, such as occurs in Landau damping. To initialize the computations in this case, the phase plane may be covered with a grid having mesh sizes Δx and Δv. A weighted particle is then located at each grid point, with a charge and mass proportional to the local value of the initial phase density. This initialization technique, which does not introduce any random fluctuations in the simulation plasma, is an example of a quiet start. We observe, however, that the particles now form a set of discrete small beams, which are subject to instabilities having growth rates proportional to $k\Delta v$, where k is the wave number [6]. Thus, while the simulation plasma is initially quiet, it may be affected by growing spurious oscillations.

An alternate approach to the computational study of collisionless plasmas is provided by numerical solutions of the Vlasov equation [7–12]. Let L denote the periodicity length of the plasma and ω_p the plasma frequency. Distances will be measured in units of L and times will be measured in units of ω_p^{-1}. It follows that the electric field is measured in units of $mL\omega_p^2/e$ where e and m are the electron charge and mass. The one-dimensional Vlasov equation then takes the form

$$(\partial f/\partial t) + v(\partial f/\partial x) - E(\partial f/\partial v) = 0, \tag{1}$$

where $f(x, v, t)$ denotes the electron distribution function and $E(x, t)$ is the electric field. Let $E(x, t) = E^{\text{ext}}(x, t) + E^{\text{int}}(x, t)$, where E^{ext} is an external electric field

and E^{int} is the internal field due to electrons and the positively charged background. The internal field is determined by Poisson's equation

$$\frac{\partial E^{\text{int}}}{\partial x} = 1 - \int_{-\infty}^{+\infty} f\, dv. \tag{2}$$

The solutions of the Vlasov equation obey the principle of conservation of density in phase. The density in phase is the distribution function itself in the present case. Let (x_0, v_0) denote the coordinates of a particle in the phase plane at time t_0. At time t, the particle has moved to the phase point (x, v). Conservation of density in phase requires $f(x, v, t) = f(x_0, v_0, t_0)$.

An important property of the solutions of the Vlasov equation is their tendency to acquire increasingly fine structures in phase plane as time increases. This phenomenon may be illustrated in terms of the oscillations of an electron gas trapped in the potential trough of an external electric field of the form

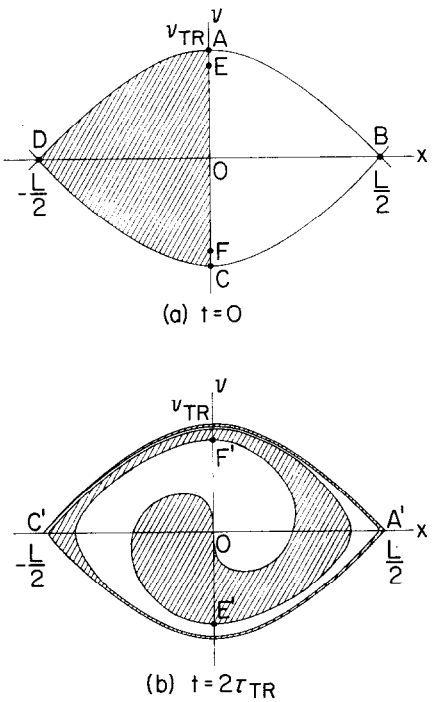

FIG. 1. Example of the development of fine structures in the solutions of the Vlasov equation.

$E = E_0 \sin 2\pi x/L$. Neglecting the internal field which would not change the results qualitatively, the electron trajectories are given by Jacobi elliptic functions,

$$\sin(\pi x/L) = \kappa\, sn(u, \kappa),$$
$$v/v_{TR} = \kappa\, cn(u, \kappa),$$

with $u = 2\pi t/\tau_{TR} + u_0$. Here τ_{TR} denotes the trapping period and v_{TR} the trapping velocity. The modulus κ and the constant u_0 depend on the initial electron coordinates in the phase plane. The limit cycle defining the boundary between trapped and untrapped electrons in the phase plane is shown in Fig. 1. If the electrons are initially distributed uniformly over the shaded area shown in Fig. 1(a), their phase density at $t = 2\tau_{TR}$ will be uniformly distributed over the shaded area shown in Fig. 1(b). In the present case, the development of the fine spiral structure near the limit cycle is caused by the sharp amplitude dependence of the period of oscillations of trapped electrons in this region. As time increases, the description of the distribution function requires an ever finer resolution which ultimately exceeds the finite capacity of computer storage.

This phenomenon has been discussed by Lynden-Bell [13] in relation to the approach to equilibrium of solutions of the Vlasov equation. When the structure becomes so fine that its scale is much smaller than the characteristic lengths and velocities of the plasma phenomena of interest, its description may be abandoned and a *coarse-grained* distribution function $\tilde{f}(x, v, t)$ defined by averaging $f(x, v, t)$,

$$\tilde{f}(x, v, t) = \int_0^1 \int_{-\infty}^{+\infty} w_x(x')\, w_v(v')\, f(x + x', v + v', t)\, dx'\, dv'. \tag{3}$$

The weight functions $w_x(x)$ and $w_v(v)$ define the resolution and the exact form of the averaging operation. The choice of these functions is an important consideration in numerical solutions of the Vlasov equation.

By reversing the sign of t in Eq. (1) it may be observed that solutions of the Vlasov equation are reversible. However, the averaging operation defined by (3) amounts to neglecting some of the information contained in the fine structure of $f(x, v, t)$. Thus numerical solutions of the Vlasov equation using this averaging operation are not exactly reversible. Since the computation of the coarse-grained distribution function also involves the averaging of different neighboring values of the original distribution function, the principle of conservation of density in phase no longer applies exactly to the coarse-grained distribution function.

2. Algorithm

The hybrid solution algorithm is presented by first considering a numerical solution of the Vlasov equation. According to the principle of conservation of

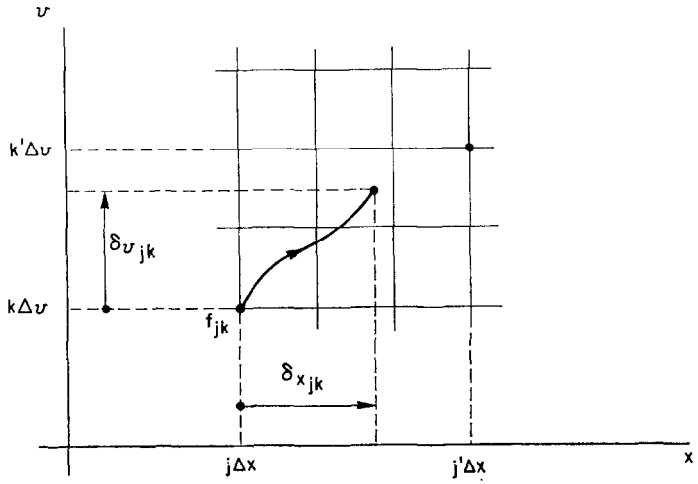

FIG. 2. Characteristics of Vlasov equation in phase plane.

density in phase, an exact solution of the Vlasov equation may be written formally as

$$f(x + \delta x, v + \delta v, t + \Delta t) = f(x, v, t) \tag{4}$$

in which δx and δv are the position and velocity increments during the time interval Δt of a particle located at (x, v) at time t. The phase plane is covered with a rectangular grid with mesh sizes Δx and Δv as shown in Fig. 2. The grid extends from $-v_{\max}$ to $+v_{\max}$ and the value of $v_{\max}$ is chosen large enough so that the grid covers all significant portions of the phase plane.

The position and velocity increments are computed by considering sample particles of masses $f(x_j, v_k, t)$ located at the grid points (x_j, v_k), and computing their position and velocity increments δx_{jk} and δv_{jk} during the time interval Δt. The sample particle locations in the phase plane at $t + \Delta t$ no longer correspond to grid points and the distribution function must be reconstructed at that time by distributing the mass of each sample particle among the neighboring grid points,

$$\begin{aligned} \hat{f}(x_{j'}, v_{k'}, t + \Delta t) = \sum_{j,k} & f(x_j + \delta x_{jk}, v_k + \delta v_{jk}, t + \Delta t) \\ & \times w_x(x_{j'} - x_j - \delta x_{jk})\, w_v(v_{k'} - \delta v_{jk}). \end{aligned} \tag{5}$$

Applying this operation to the solution of Vlasov's equation (4) yields

$$\begin{aligned} \tilde{f}(x_{j'}, v_{k'}, t + \Delta t) = \sum_{j,k} & f(x_j, v_k, t) \\ & \times w_x(x_{j'} - x_j - \delta x_{jk})\, w_v(v_{k'} - v_k - \delta v_{jk}). \end{aligned} \tag{6}$$

The weight functions w_x and w_v determine what fraction of the mass of a sample particle is assigned to each neighboring grid point. The discrete sum in Eq. (5) defines an averaging operation similar to Eq. (3). In the present method the averaging operation must be carried out by a discrete sum instead of an integral since the phase plane itself has been discretized by the introduction of a grid. Weight functions for which the averaging operation conserves any finite number of moments are derived in Section 3. It is not possible, however, to derive functions w_x and w_v for which all moments of the distribution function are conserved, as is done in the Fourier–Fourier transform method [11, 18]. This results in some diffusion of the distribution function in the phase plane with rates which are estimated in Section 3.

The evaluation of the position and velocity increments δx_{jk} and δv_{jk} of the sample particles is presented in Appendix A. The method uses an area weighting scheme and is based on a Lagrangian formulation of particle dynamics in which energy is conserved [19].

In a number of problems of physical interest, the initial distribution function consists of several relatively cold beams and only a fraction of the phase plane is occupied by particles. As the solution proceeds in time, the principle of conservation of density in phase (which is still approximately satisfied by the numerical solution) requires that this fraction must remain constant. Where no particles are present, the distribution function is zero and does not need to be advanced. This is achieved in the code by setting a threshold value (for example 10^{-5} times the maximum value of the distribution function) below which no sample particle is considered. The electric potential is computed by Fourier transforms so that the electron density is automatically renormalized at each time step. Thus, the slight loss of particles resulting from a finite threshold does not result in the build up of a net charge in the plasma. This feature of the direct method of integration of the Vlasov equation, which has no counterpart in transform methods, may yield a considerable saving of computing time when multidimensional problems are considered.

It is not necessary to reconstruct the distribution function by the averaging operation (6) for every time step at which the electric field is computed. If Δt is the time step used to advance the sample particles, the electric field needs to be computed after each Δt increment, but the distribution function can be reconstructed only every $N\Delta t$, where N is a properly chosen integer. In addition to saving computing time, this procedure reduces the diffusion in phase plane caused by application of the averaging operation.

The Vlasov solution described above in which the distribution function is reconstructed only every N-th time step begins to resemble particle simulations and it seems appropriate to call it a "hybrid" solution. As noted in the introduction, particle simulations in which weighted particles are loaded on an (x, v) grid to

represent the initial distribution function have been used [5]. In particle simulation, however, the distribution function is never reconstructed ($N = \infty$) and the simulation plasma is subject to beaming instabilities. An evaluation of the amplitudes and growth rates of these instabilities, based on Dawson's theory [6], is presented in Section 5. This evaluation shows that beaming instabilities have particularly strong effects on particle simulations after a time $2\pi/k_{\max}\Delta v$, where $k_{\max}$ is the maximum wavenumber retained in the solution. By reconstructing the distribution function at time intervals which are short compared to $2\pi/k_{\max}\Delta v$, the simulation plasma is forced to behave as a continuum and no beaming instabilities can develop.

Examples of numerical solutions involving two-stream instabilities are presented in Section 4. These examples confirm that it is possible to minimize the effects of both beaming instabilities and diffusion by properly choosing the frequency of reconstruction of the distribution function.

3. Weight Functions

To derive weight functions $w_x(x)$ and $w_v(v)$ for which the averaging operation defined by Eq. (5) conserves a finite number of moments it is sufficient to consider the one-dimensional operation

$$\tilde{f}(v_{j'}) = \sum_j f(v_j + \delta v_j)\, w(v_{j'} - v_j - \delta v_j). \tag{7}$$

The weight functions thus found will be applicable to either coordinate or velocity. Such weight functions, conserving zeroth, first and second order moments have been derived by K-W Li [8].

a. *Moment Conservation Conditions*

The moment of order n before averaging is

$$\langle v^n \rangle = \sum_j (v_j + \delta v_j)^n f(v_j + \delta v_j). \tag{8}$$

After averaging the same moment becomes

$$\langle \tilde{v}^n \rangle = \sum_{j'} v_{j'}^n \tilde{f}(v_{j'}). \tag{9}$$

Substituting (7) into (9) and reversing the order of the sums over j and j' yields

$$\langle \tilde{v}^n \rangle = \sum_j f(v_j + \delta v_j) \sum_{j'} v_{j'}^n w(v_{j'} - v_j - \delta v_j).$$

The moments (8) and (9) are therefore equal if the equality

$$\sum_{j'} v_{j'}^n w(v_{j'} - v_j - \delta v_j) = (v_j + \delta v_j)^n \tag{10}$$

holds for all values of $v_j + \delta v_j$.

b. *Derivation of Weight Functions*

Let $k = j' - j$, since the variable v is represented on a grid with mesh size Δv we have $v_{j'} = (j + k)\,\Delta v$, $v_{j'} - v_j = k\Delta v$ and $v_j = j\Delta v$. The moment condition (10) becomes

$$\sum_k (j + k)^n\, w[(k - p)\,\Delta v] = (j + p)^n, \tag{11}$$

where $p = \delta v_j/\Delta v$. We may assume without loss of generality that δv_j is positive and smaller than the mesh size Δv so that $0 \leqslant p < 1$. The function $w(v)$ is now assumed to be even and to extend over Q meshes Δv on either side of the origin. The condition (11) is satisfied if

$$\sum_{k=1-Q}^{Q} k^m w[(k - p)\,\Delta v] = p^m \tag{12}$$

for $m = 0, 1, \ldots, n$. All moments up to order n will then be conserved.

We first assume that n is odd and set $Q = (n + 1)/2$. Consider the Lagrangian interpolation with $n + 1$ points of the function p^m. Since $m \leqslant n$, the interpolation is exact and we have [20]

$$\sum_{k=1-Q}^{Q} k^m A_k^{(n+1)}(p) = p^m, \tag{13}$$

in which the functions $A_k^{(n+1)}(p)$ for $1 - Q \leqslant k \leqslant Q$ and $0 \leqslant p \leqslant 1$ are the Lagrangian coefficients with $n + 1$ points. Comparing (12) and (13) yields the desired weight function,

$$w[(k - p)\,\Delta v] = A_k^{(n+1)}(p),$$

or

$$w(v) = A_k^{(n+1)}\left(k - \frac{v}{\Delta v}\right), \qquad \text{for} \quad (k - 1)\,v \leqslant v \leqslant k\,\Delta v \tag{14}$$

with $k = (1 - n)/2, \ldots, (1 + n)/2$. For n even, we set $Q = 1 + n/2$. The Lagrangian

coefficients in this case do not yield even weight functions. Even weight functions may, however, be obtained by symmetrization as follows,

$$w(v) = \begin{cases} \frac{1}{2} A^{(n+1)}_{-(n/2)} \left(1 + \frac{n}{2} + \frac{v}{\Delta v}\right) & -\left(\frac{n}{2}+1\right)\Delta v \leqslant v \leqslant -\frac{n}{2}\Delta v, \\ \frac{1}{2}\left[A^{(n+1)}_{k}\left(k - \frac{v}{\Delta v}\right) + A^{(n+1)}_{1-k}\left(1 - k + \frac{v}{\Delta v}\right)\right] & (k-1)\Delta v \leqslant v \leqslant k\,\Delta v, \\ \frac{1}{2} A^{(n+1)}_{-(n/2)}\left(1 + \frac{n}{2} - \frac{v}{\Delta v}\right) & \frac{n}{2}\Delta v \leqslant v \leqslant \left(\frac{n}{2}+1\right)\Delta v, \end{cases} \tag{15}$$

with $k = 1 - n/2, \ldots, n/2$.

c. *Examples*

For $n = 1$ the averaging operation (7) conserves particles and momentum. Since n is odd, Eq. (14) is applicable and we have

$$w^{(1)}(v) = A^{(1)}_1[1 - (v/\Delta v)] = 1 - (v/\Delta v)$$

for $0 \leqslant v \leqslant \Delta v$. In the interval $-\Delta v \leqslant v \leqslant 0$, the function $w^{(1)}(v)$ is defined by symmetry and it is zero for $|v| > \Delta v$. This function is illustrated at (a) in Fig. 3. For $n = 2$ the averaging operation conserves particles, momentum and energy. Since n is even, we apply Eqs. (15),

$$w^{(2)}(v) = \begin{cases} \frac{1}{2}\left[A^{(3)}_1\left(1 - \frac{v}{\Delta v}\right) + A^{(3)}_0\left(\frac{v}{\Delta v}\right)\right] = 1 - \frac{v}{\Delta v} + \frac{1}{4}\frac{v}{\Delta v}\left(1 - \frac{v}{\Delta v}\right) & \text{for} \quad 0 \leqslant v \leqslant \Delta v \\ \frac{1}{2} A^{(3)}_{-1}\left(2 - \frac{v}{\Delta v}\right) = \frac{1}{4}\left(2 - \frac{v}{\Delta v}\right)\left(1 - \frac{v}{\Delta v}\right) & \text{for} \quad \Delta v \leqslant v \leqslant 2\Delta v. \end{cases}$$

This function is illustrated at (b) in Fig. 3, it extends over four meshes and has negative side lobes. The fifth degree weight function $w^{(5)}(v)$ is illustrated at (c) in Fig. 3. This function extends over six meshes and has negative and positive side lobes reminiscent of the weight function $\sin(\pi v/\Delta v)/(\pi v/\Delta v)$ used in the Fourier–Fourier transform method [11, 18].

Most of the computations presented in Section 4 are based on the quadratic weight function $w^{(2)}(v)$ for $w_x(x)$ and $w_v(v)$. However, some computations using linear and fifth-degree weight functions are also presented.

The negative sidelobes in the quadratic and higher-order weight functions tend to produce small ripples in the reconstructed distribution function. This effect is similar to the Gibbs phenomenon in Fourier transforms and for small values of the

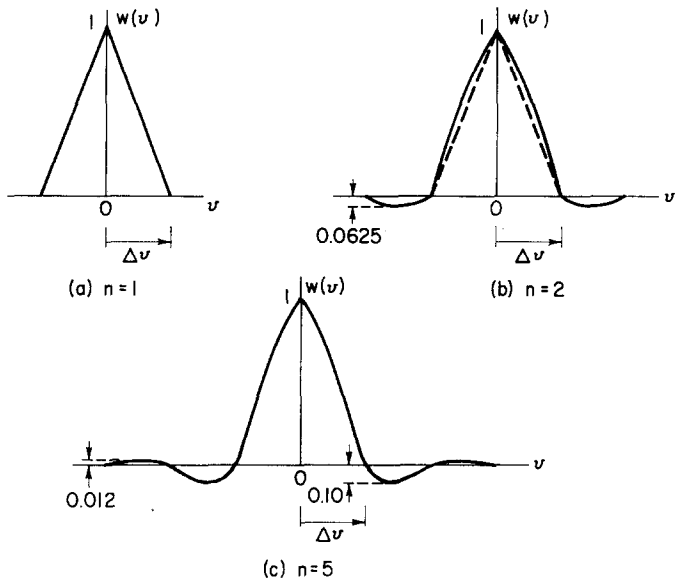

FIG. 3. Examples of weight functions for averaging of the distribution in phase plane.

distribution function may give local negative values. The scale and amplitude of these ripples remain negligible if the mesh sizes are kept small compared to the local characteristic lengths and velocities of the plasma phenomena being considered.

d. *Diffusion Rates*

After the sample particles have been advanced N time steps, their velocities are v_j and the microscopic velocity distribution function is

$$f(v) = \sum_j f_j \delta(v - v_j).$$

At this time the distribution function is reconstructed, using the weight function $w(v)$, and the coarse-grained distribution function is

$$\tilde{f}(v) = \sum_j f_j w(v - v_j)/\Delta v.$$

To determine what features of the function $f(v)$ are lost when it is replaced by $\tilde{f}(v)$, consider the Fourier transforms of both functions, called characteristic functions of the distributions [14],

$$H(q) = \int_{-\infty}^{+\infty} f(v)\, e^{iqv}\, dv = \sum_j f_j e^{iqv_j}, \tag{16}$$

and

$$\tilde{H}(q) = \int_{-\infty}^{+\infty} \tilde{f}(v)\, e^{iqv}\, dv = W(q) \sum_j f_j e^{iqv}. \tag{17}$$

Here the function $W(q)$ denotes the Fourier transform of the weight function $w(v)/\Delta v$. Plots of $W(q)$ for linear and quadratic weight functions are shown in Fig. 4.

Comparing Eqs. (16) and (17) yields

$$\tilde{H}(q) = H(q)\, W(q). \tag{18}$$

The reconstruction of the distribution function, therefore, appears as a smoothing operation in phase space. Values of H corresponding to low values of q represent large-scale features of the distribution function and should be left unchanged. However, values of H corresponding to high values of q, which represent fine structures of the distribution function are suppressed.

To estimate diffusion rates, consider the quantity

$$D(q) = 1 - W(q).$$

After m reconstructions, the Fourier transform of the distribution function is

$$\tilde{H}(q, m) = H(q, m = 0)[1 - D(q)]^m.$$

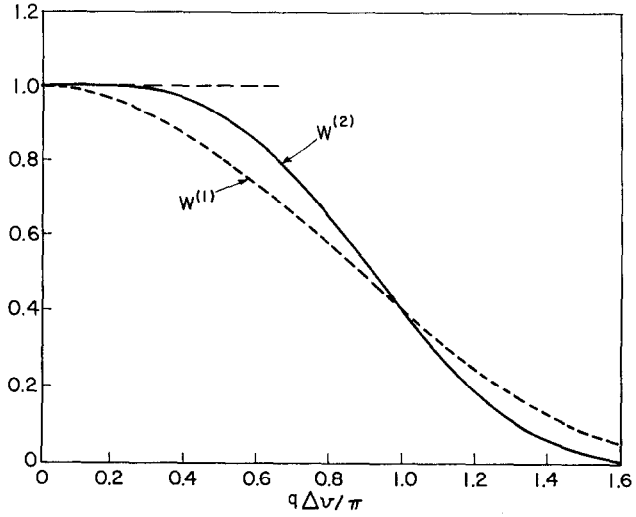

FIG. 4. Fourier transforms of the weight functions $w^{(1)}$ and $w^{(2)}$.

Assuming $D(q) \ll 1$, which is valid for $q\Delta v/\pi \ll 1$, this relation yields

$$\tilde{H}(q, m) = H(q, m = 0)\, e^{-mD(q)}. \tag{19}$$

Thus the quantity $D(q)$ represents the diffusion rate of a feature of scale $2\pi/q$. Values of $D(q)$ corresponding to linear and quadratic weight functions are given in Table I. For example, a feature with characteristic velocity $v_c = 10\Delta v$, for which $q\Delta v/\pi = 0.2$, has a diffusion rate $D^{(2)}(q\Delta v/\pi = 0.2) = 2.5 \times 10^{-3}$ corresponding to the quadratic weight function. The distribution function can, therefore, be reconstructed 400 times before this feature is reduced by an e-fold. In the case of beaming instabilities, the velocity scale is of the order of Δv, i.e., $q\Delta v/\pi \simeq 1$. We observe in Fig. 4 that $D^{(2)}(q\Delta v/\pi = 1) = 0.4$ and features at this scale are suppressed after a few reconstructions of the distribution function.

TABLE I

Diffusion Rates for Linear and Quadratic Weight Functions

$q\Delta v/\pi$	0	0.1	0.2	0.3	0.4
$D^{(1)}$	0	0.0082	0.0325	0.0719	0.1249
$D^{(2)}$	0	0.0002	0.0025	0.0120	0.0353

Note that the diffusion rates for $q\Delta v/\pi \ll 1$ may be related to the moments of the weight function $w^{(n)}(v)$ by expanding $W^{(n)}(q)$ in Taylor series near $q = 0$. We have for n odd

$$\begin{aligned} D^{(n)}(q) &= -\frac{q^{n+1}}{(n+1)!} \frac{d^{n+1}W^{(n)}}{dq^{n+1}}\bigg|_{q=0} \\ &= (-1)^{(n-1)/2} \frac{q^{n+1}}{(n+1)!} \langle v^{n+1} \rangle^{(n)}, \end{aligned} \tag{20}$$

where $\langle v^r \rangle^{(n)}$ denotes the moment of order r of the weight function $w^{(n)}(v)$. This relation shows that weight functions which conserve a larger number of moments yield less diffusion. For n even, the first non-zero moment is of order $n + 2$.

The estimate of the diffusion rates given in this section does not take into account the discrete nature of the grid used to represent the phase plane in the present method. A more complete analysis of the diffusion process, given in Appendix B, shows that the above estimate gives the average diffusion rates assuming that the sample particles, before reconstruction of the distribution function, are located at random with uniform probability between grid points.

4. Examples

Case 1: *Two-Stream Instability with Equal Beams*

Consider a two-stream instability resulting from the initial conditions defined by the distribution function

$$f(x, v, t = 0) = f_0(v)[1 + 2\epsilon \cos 2\pi x],$$

with

$$f_0(v) = (1/v_{th}^3 \sqrt{2\pi})\, v^2 e^{-v^2/2v_{th}^2},$$

and $v_{th} = 0.3/\pi$, $\epsilon = 2.5\ 10^{-2}$. These initial conditions correspond to a system length $L = 10.5\lambda_D$ where $\lambda_D = v_{th}/\omega_p$ is the Debye Length. The initially excited mode has a wavelength equal to the length of the system, i.e., corresponds to the first mode. The linear growth rates for this problem have been computed by Grant and Feix [17]. The first mode is the only unstable mode and has a growth rate $\gamma = 0.24$.

The electrostatic energy for four solutions of this problem is shown in Fig. 5. All four curves correspond to the same maximum velocity, $v_{\max} = 4.2v_{th}$, the same mesh sizes, $\Delta x = 1/32$ and $\Delta v = 2v_{\max}/120$ and the same time step $\Delta t = 0.2$. The threshold, i.e., the minimum value of the distribution function for which a sample particle is considered, was set to zero.

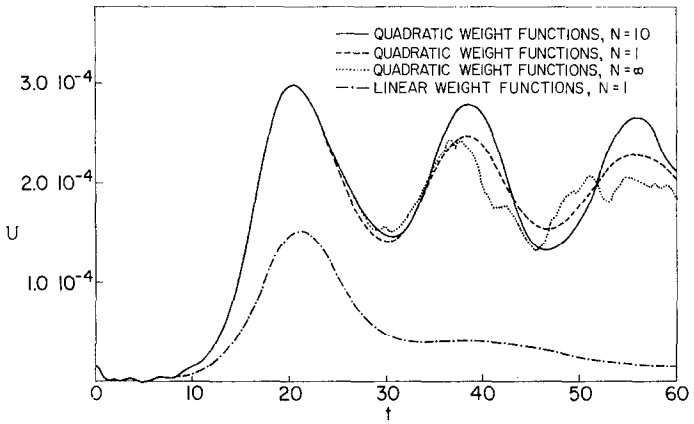

FIG. 5. Electrostatic energy for two-stream instability with equal beams.

The solid curve corresponds to a reconstruction of the distribution function every ten time steps, using quadratic weight functions. The broken line corresponds to a reconstruction of the distribution function at every time step, also using

quadratic weight functions. We observe in this case a decrease in the amplitude of trapping oscillations. This is attributed to a diffusion of the distribution function in phase plane due to repeated applications of the averaging operation defined by Eq. (5). Note that although energy is conserved in the averaging operation, higher moments are not conserved. This tends to flatten the distribution function resulting in the escape of trapped particles. The curve drawn with dashes and dots in Fig. 5 corresponds again to a reconstruction of the distribution function at every time step. This time, however, linear weight functions were used. The distribution function flattens rapidly in this case, filling the hole located at the center of the trapping region.

Because of the rather long tails in the distribution function in the present problem, particles are lost over the boundaries at $v = \pm v_{\max}$. For both solutions with quadratic weight functions, the relative particle loss is 4×10^{-4}. After corrections for particles lost over the boundary, the relative energy error is 5.5×10^{-5}. For the solution with linear weight functions, the relative particle loss is 2.7×10^{-3} and the relative energy error after correction for lost particles is 6.2×10^{-2}.

A Vlasov solution for this example has been carried out by Denavit and Kruer [18] using the Fourier–Fourier transform method. The electrostatic energy for this solution is in good agreement with the solid curve in Fig. 5. Particle simulations have also been carried out by Armstrong and Nielson [12] and by Denavit and Kruer [18]. The results of these simulations also agree with the result of the present solution.

An additional computation was carried out in which the distribution function was never reconstructed. The code then operated as a particle code with particles of different masses initially arranged in a regular array in the phase plane. Phase plots for this run showed beaming instabilities starting to appear at $t = 10$. The total electrostatic energy for this case is represented by the dotted curve in Fig. 5. We observe that spurious oscillations appear after $t \simeq 28$.

Case 2: Two-Stream Instability with Unequal Beams

Consider now an instability resulting from the interaction of a small beam with a Maxwellian plasma. The initial conditions are

$$f(x, v, t = 0) = f_0(v)\left(1 + 2\epsilon \sum_{n=1}^{21} n \cos(2\pi n x + \phi_n)\right),$$

with

$$f_0(v) = (1/\sqrt{\pi}\, v_p)(n_p e^{-v^2/v_p^2} + n_b e^{-(v-v_d)^2/v_b^2}),$$

and $v_p = \sqrt{2}\, 10^{-2}$, $v_d = 2.6 v_p$, $v_b = 0.25 v_p$, $n_p = 0.95$, $n_b = 0.05$, $\epsilon = 2.5 \times 10^{-4}$ and initial phases ϕ_n chosen at random. Thus the small beam contains 5% of the

plasma and its mean velocity is 3.66 thermal velocities. These initial conditions correspond to a system length of $100\lambda_D$.

The total electrostatic energy for three solutions of this problem is shown in Fig. 6. All three curves correspond to the same maximum velocity $v_{\max} = 4v_p$, velocity interval $\Delta v = 2v_{\max}/120$ and time step $\Delta t = 0.2$ with the distribution function reconstructed every 10 time steps. A threshold equal to 10^{-5} times the maximum value of the distribution function was set. Below this threshold no sample particles were considered.

Note that the present case involves five trapping regions (the fifth mode is the most unstable mode) so that smaller values of Δx should be considered than in the previous case. The solid line in Fig. 6 corresponds to $\Delta x = 1/128$ with quadratic weight functions. The broken line corresponds to $\Delta x = 1/64$, again using quadratic weight functions. The amplitude of trapping oscillations is reduced in this case. The curve drawn with dashes and dots in Fig. 6 corresponds to $\Delta x = 1/64$ using fifth-degree weight functions. We observe that the use of higher-order weight functions tends to reduce the diffusion of the distribution function in phase space.

The relative particle loss with $\Delta x = 1/128$ and quadratic weight functions is 4×10^{-6} and the relative energy error is 3.5×10^{-4}. Comparable values of the particle loss and energy error are found in the other two computations.

The density in phase near saturation is shown in Fig. 7. Numbers from 1 to 9 indicate relative densities. Blanks correspond to densities which are less than one-tenth of the maximum density. Negative signs correspond to negative values of the density larger in magnitude than one-tenth of the maximum density.

Particle simulations have been carried out for this example by Morse and Nielson [3] and Denavit and Kruer [18]. The results of Morse and Nielson agree

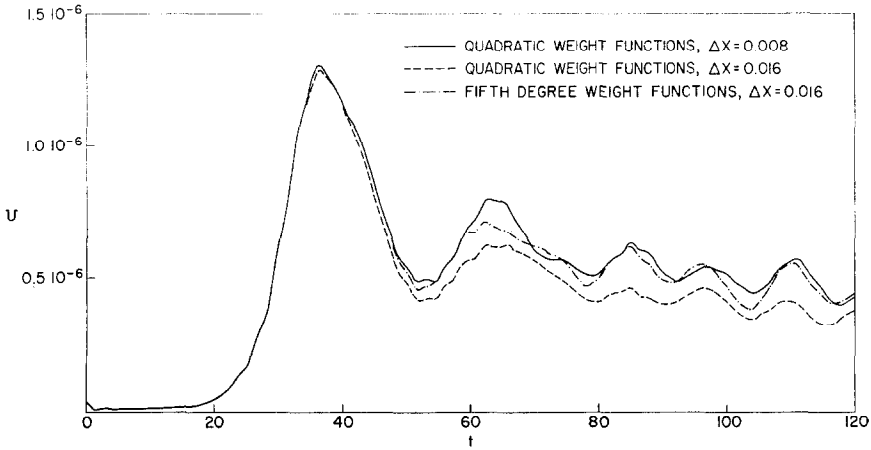

FIG. 6. Electrostatic energy for two-stream instability with unequal beams.

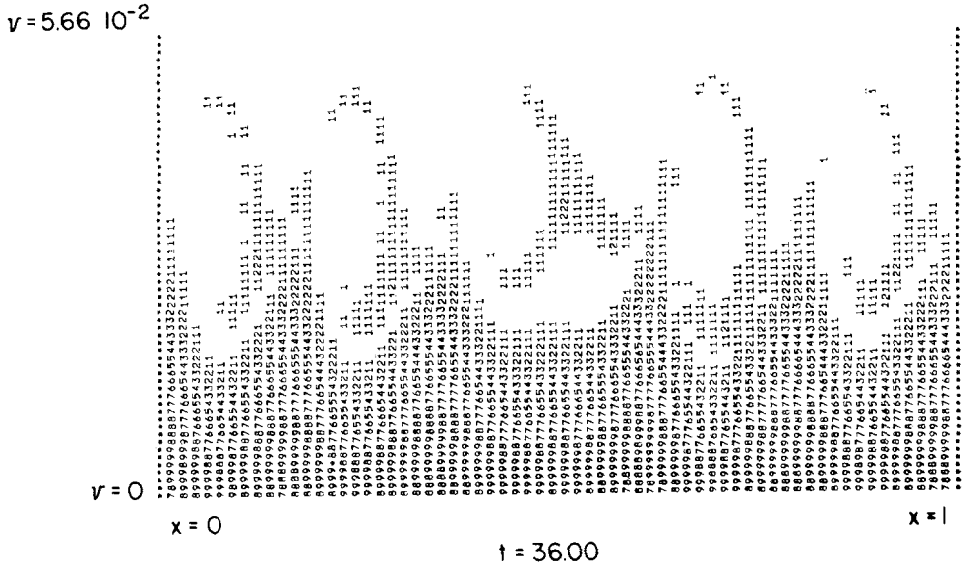

FIG. 7. Density in phase near saturation for two-stream instability with unequal beams.

only qualitatively with the present Vlasov solution. The differences, however, may be attributed to the longer periodicity length considered by these authors and the random nature of their initial conditions. The results obtained using Kruer's finite-size particle code with a quiet start [18] agree quantitatively with the present solution out to $t \simeq 70$, after which the two solutions remain in qualitative agreement.

The present method has been applied to several other one-dimensional problems including an echo, a sideband instability and an investigation of trapping effects on the propagation of wave packets.

The smoothing operation may be generalized to apply to nonuniform and time-varying mesh sizes, which would allow a concentration of the computer capacity in the most significant regions of phase space. These generalizations, and the conservation of density in phase space discussed in Section 2, are important considerations in the potential applications of hybrid solutions to multidimensional problems.

5. BEAMING INSTABILITY

The time interval between reconstructions of the distribution function may be estimated in terms of Dawson's theory of plasma oscillations of electron beams [6]. Consider a one-dimensional system of electron beams with velocities $V_\sigma = \sigma \Delta v$

and densities $N_\sigma = N(V_\sigma)\,\Delta v$, with $\sigma = 0, \pm 1, \pm 2, \ldots$, moving over a neutralizing positively charged background. Let $n_\sigma(x, t)$ and $v_\sigma(x, t)$ denote perturbations in density and velocity for each beam. The linearized equations of motion and continuity for each beam and Poisson's equation yield

$$(\partial v_\sigma/\partial t) + V_\sigma(\partial v_\sigma/\partial x) = -(eE/m),$$
$$(\partial n_\sigma/\partial t) + N_\sigma(\partial v_\sigma/\partial x) + V_\sigma(\partial n/\partial x) = 0,$$
$$\frac{\partial E}{\partial x} = -4\pi e \sum_\sigma n_\sigma .$$

Assuming solutions of the form $A(x, t) = A(\omega, k)\, e^{-i(\omega t - kx)}$ for the perturbation quantities yields

$$n_\sigma(\omega, k) = (4\pi e^2/m)[N_\sigma/(\omega - kV_\sigma)^2], \tag{21}$$
$$v_\sigma(\omega, k) = (4\pi e^2/m)[1/k(\omega - kV_\sigma)], \tag{22}$$
$$E(\omega, k) = -(4\pi e i/k), \tag{23}$$

with the dispersion relation

$$\frac{4\pi e^2}{m} \sum_\sigma \frac{N_\sigma}{(\omega - kV_\sigma)^2} = 1. \tag{24}$$

Dawson has shown that for $\Delta v \to 0$, the left member of Eq. (24) may be written as the sum of an integral and a singular term. For a Maxwellian beam density distribution $N(V_\sigma) = (n_0/\sqrt{2\pi}\, v_{th}) \exp(V_\sigma^2/2v_{th}^2)$, the dispersion relation becomes

$$(4\pi^2/\sqrt{2\pi})(v_{th}/\Delta v)\, e^{-\zeta^2} e^{\pm 2\pi i \omega/k\Delta v} = 1 + k^2\lambda_D^2 + \zeta Z(\zeta), \tag{25}$$

where $Z(\zeta)$ is the plasma dispersion function with $\zeta = \omega/\sqrt{2}kv_{th}$. The positive sign is to be used in Eq. (25) for Im $\omega > 0$ and the negative sign for Im $\omega < 0$. For each k, Eq. (25) has two complex conjugate roots corresponding to each beam. Letting $\omega_\sigma = \alpha_\sigma + i\beta_\sigma$ and $\zeta_\sigma = \sigma\Delta v/\sqrt{2}v_{th}$ yields

$$\alpha_\sigma = \frac{k\,\Delta v}{2\pi} \tan^{-1}\left(\frac{\zeta_\sigma \text{ Im } Z(\zeta_\sigma)}{1 + k^2\lambda_D^2 + \text{Re } Z(\zeta_\sigma)}\right) + k\sigma\,\Delta v, \tag{26}$$

and

$$\beta_\sigma = \pm(k\,\Delta v/2\pi)(\ln(4\pi^2 v_{th}/\sqrt{2\pi}\,\Delta v) - \zeta_\sigma^2$$
$$- (1/2)\ln\{[1 + k^2\lambda_D^2 + \zeta_\sigma \text{ Re } Z(\zeta_0)]^2 + [\zeta_\sigma \text{ Im } Z(\zeta_\sigma)]^2\}). \tag{27}$$

Equations (21) and (22) are normal modes for a given k and satisfy the normalization relation

$$\sum_\sigma \frac{1}{2N_\sigma}(\omega + \omega' - 2kV_\sigma)\, n_\sigma(\omega, k)\, n_\sigma(\omega', k) = \begin{cases} 0 & \text{for } \omega \neq \omega', \\ H(\omega, k) & \text{for } \omega = \omega'. \end{cases} \tag{28}$$

For $\Delta v \to 0$ and a Maxwellian beam distribution the function $H(\omega, k)$ reduces to

$$H(\omega_\sigma, k) = \mp(2\pi i/k\,\Delta v)\{1 + (1/k^2\lambda_D^2)[1 + \zeta_\sigma Z(\zeta_\sigma)]\}. \tag{29}$$

To verify that the instability occurring in the present method, when the distribution function is not reconstructed, is indeed a beaming instability, a computation was carried out for a Maxwellian beam distribution with $v_{th} = 0.1$ and $\Delta v = 0.02$. An initial density perturbation was applied to the central beam,

$$n_\sigma(x, t = 0) = \begin{cases} \epsilon N_{\sigma=0} \cos kx & \text{for } \sigma = 0, \\ 0 & \text{for } \sigma \neq 0. \end{cases} \tag{30}$$

with $\epsilon = 0.0025$ and $k\lambda_D = \pi/5$. No initial velocity perturbation was applied. The central beam velocity at $x = \pi/2k$ from the code used in Section 4 is given by the solid curve in Fig. 8. There is a gentle growth out to $t = 46$, followed by a sign reversal at $t = 48$ and a very steep growth for $t > 48$. The electric field for this computation first drops rapidly to very low values, then suddenly reappears to reach a maximum 23 times its initial value at $t = 2\pi/k\Delta v = 50$.

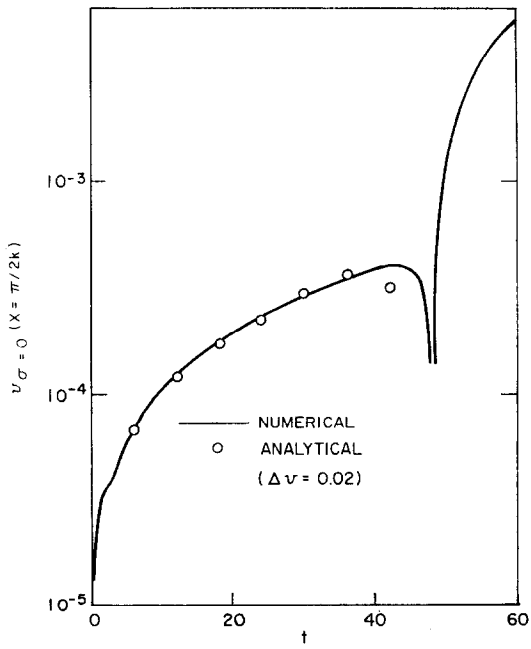

FIG. 8. Velocity perturbation of central beam for beaming instability test.

Expanding the velocity perturbation of the central beam into normal modes and using the normalization relations (28), the initial conditions (30) yield

$$\frac{v_{\sigma=0}}{\Delta v} = \frac{\omega_p{}^2\epsilon}{(2\pi)^{3/2}} \frac{\Delta v}{v_{th}} k^2\lambda_D{}^2 \sin kx \sum_\sigma \frac{\pm e^{-i\omega_\sigma t}}{\omega_\sigma{}^2[1 + k^2\lambda_D{}^2 + \zeta_\sigma Z(\zeta_\sigma)]} . \tag{31}$$

The terms of the sum in Eq. (31) oscillate with the frequencies α_σ given by Eq. (26) approximately equal to the Doppler frequencies $k\sigma\Delta v$ of the beams and grow exponentially with growth rates β_σ given by Eq. (27). The damped terms corresponding to the negative sign in Eq. (27) are ignored. The expression in brackets in the denominator of Eq. (31) is the Landau denominator which in the present case has a minimum near $\zeta_\sigma = 1.8$. Thus, the dominant terms of the sum in Eq. (31) occur for $\sigma \simeq 0$, which corresponds to the minimum of $\omega_\sigma{}^2$ and

$$\sigma \simeq \pm(1.8)\sqrt{2}v_{th}/\Delta v \simeq 13$$

which corresponds to the minimum of the Landau denominator.

For $t < 2\pi/k\Delta v = 50$, the terms corresponding to $\sigma \simeq \pm 13$ phase mix and the behavior of the velocity perturbation $v_{\sigma=0}$ is given by the terms near $\sigma = 0$. The growth rates for these terms is $\beta_{\sigma=0} = 0.08$. The circles in Fig. 8 give values computed by taking $\sigma = 0, \pm 1, \pm 2$. These values are in good agreement with the computer results represented by the solid curve.

The growth rate for the terms corresponding to $\sigma \simeq \pm 13$ is $\beta_{\pm 13} = 0.06$. For $t \simeq 2\pi/k\Delta v = 50$ these terms no longer phase mix. By this time they have grown by a factor of approximately 20 and therefore give rise to a strong echo. This is evident in the solid line in Fig. 8 for $t > 48$, and also agrees with the electric field results which show a sudden regrowth with a maximum at $t = 50$ which is 23 times the initial electric field.

APPENDIX A: Position and Velocity Increments

Let $f_{jk} = f(x_j, v_k, t_0)$ denote the value of the distribution function at the grid point (x_j, v_k) at time t_0 and let $\delta x_{jk}(t)$ denote the displacement of the sample particle of mass f_{jk} located at (x_j, v_k) at time t_0. The position and velocity increments δx_{jk} and $\delta v_{jk} = \delta \dot{x}_{jk}$ will be computed as functions of time using a Lagrangian formulation derived by R. Lewis [19]. This formulation yields an algorithm for advancing sample particles which conserves energy independently of the mesh size Δx.

a. *Lagrangian Formulation*

The electrostatic potential $\psi(x, t)$ is defined in terms of a base function $\phi(x)$ and a set of time-dependent coefficients $\alpha_j(t)$ by the linear combination

$$\psi(x, t) = \sum_{j=0}^{J-1} \alpha_j(t)\, \phi(x - x_j). \tag{A1}$$

Here $x_j = j\Delta x$, for $j = 0,..., J - 1$, denote the grid-point locations and J is the number of grid points in the x direction. The Lagrangian for a system of charged particles is

$$L = \sum_{j=0}^{J-1} \sum_{k=1}^{K} \frac{1}{2} f_{jk}\, \delta\dot{x}_{jk}^2 + \sum_{j=0}^{J-1} \sum_{k=1}^{K} f_{jk} \sum_{i=0}^{J-1} \alpha_i \phi(x_j + \delta x_{jk} - x_i)$$

$$+ \int_0^1 \left\{ \frac{1}{2} \left[\sum_{j=0}^{J-1} \alpha_j \phi'(x - x_j) \right]^2 - \sum_{j=0}^{J-1} \alpha_j \phi(x - x_j) \right\} dx, \tag{A2}$$

where K is the number of grid points in velocity and $\phi'(x) = d\phi/dx$. The first term in Eq. (A2) is the kinetic energy, the second term is the negative of the interaction energy and the third term is the electrostatic energy of the system.

The equations of motion are obtained by taking variations with respect to the particle displacements δx_{jk},

$$\delta\ddot{x}_{jk} = \sum_{i=0}^{J-1} \alpha_i(t)\, \phi'(x_j + \delta x_{jk} - x_i), \tag{A3}$$

and Poisson's equation is obtained by taking variations with respect to the potential coefficients α_i,

$$\sum_{i=0}^{J-1} \alpha_i \int_0^1 \phi'(x - x_i)\, \phi'(x - x_j)\, dx$$

$$= \int_0^1 \phi(x - x_j)\, dx - \sum_{i=0}^{J-1} \sum_{k=1}^{K} f_{ik} \phi(x_i + \delta x_{ik} - x_j) \tag{A4}$$

b. *Base Function*

The specific algorithm to be used now depends on the form of the base function $\phi(x)$, which determines the charge sharing scheme to be used in advancing particles. In the present algorithm, particles having a triangular charge distribution with half-width Δx are used. The corresponding base function is

$$\phi(x) = \begin{cases} (1/2)[(3/2) + (x/\Delta x)]^2 & \text{for } -(3\Delta x/2) \leqslant x \leqslant -(\Delta x/2), \\ (3/4) - (x/\Delta x)^2 & \text{for } -(\Delta x/2) \leqslant x \leqslant +(\Delta x/2), \\ (1/2)[(3/2) - (x/\Delta x)]^2 & \text{for } (\Delta x/2) \leqslant x \leqslant (3\Delta x/2). \end{cases}$$

Let $x_{j'}$ denote the grid point location closest to the sample particle (jk) and set $p = (x_j + \delta x_{jk} - x_{j'})/\Delta x$; then $|p| \leqslant \frac{1}{2}$. When the above base function is substituted into the right member of Eq. (A3) the sum reduces to three terms and we have

$$\delta\ddot{x}_{jk} = (1/\Delta x)[-\alpha_{j'-1}(\tfrac{1}{2} - p) - 2\alpha_{j'}p + \alpha_{j'+1}(\tfrac{1}{2} + p)]. \tag{A5}$$

Substituting the base function into Eq. (A4) yields

$$(1/6\Delta x)(-\alpha_{j-2} - 2\alpha_{j-1} + 6\alpha_j - 2\alpha_{j+1} - \alpha_{j+2}) = \Delta x - \beta_j\,, \tag{A6}$$

where

$$\beta_j = \sum_{i=0}^{J-1} \sum_{k=1}^{K} f_{ik}\phi(x_i + \delta x_{ik} - x_j) \tag{A7}$$

is the charge assigned to grid point j. Note that the left member of Eq. (A6) is a finite-difference representation of the second derivative of the potential.

Since periodic boundary conditions are assumed, it is convenient to solve Poisson's equation by discrete Fourier-transforms [15, 16]. Let

$$\bar{\alpha}_n = \sum_{j=0}^{J-1} \alpha_j e^{(2\pi i/J)nj}$$

and

$$\bar{\beta}_n = \sum_{j=0}^{J-1} \beta_j e^{(2\pi i/J)nj}$$

denote the transforms of the arrays α_j and β_j. Multiplying Eq. (A6) by $\exp(2\pi inj/J)$, summing over j and solving for $\bar{\alpha}_n$ yields

$$\bar{\alpha}_n = \frac{-\bar{\beta}_n}{4J \sin^2(\pi n/J)[1 - \frac{2}{3}\sin^2(\pi n/J)]}\,.$$

The array α_j is then obtained by taking the inverse transform of $\bar{\alpha}_n$.

The time integration for the quantities δx_{jk} and α_j is carried out by a conventional leap-frog scheme. Since the distribution function requires simultaneous knowledge of the particle positions and velocities, a half-time step is taken just before and after each reconstruction of the distribution function.

The computing time to advance the sample particle was found to be approximately 0.5 msec per particle, per time step, on the CDC 3800. The computing time to reconstruct the distribution function with quadratic weight functions was approximately 0.7 msec per particle.

c. *Energy Conservation*

As a consequence of the Lagrangian formulation, the present algorithm for advancing the sample particles conserves momentum and energy independently of the mesh size Δx. The expression for the total energy is provided by the Hamiltonian

$$H = \frac{1}{2} \sum_{j=0}^{J-1} \sum_{k=1}^{K} f_{jk}\, \delta \dot{x}_{jk}^2 + \frac{1}{2} \sum_{i,j=0}^{J-1} \alpha_i \alpha_j \int_0^1 \phi'(x - x_i)\, \phi'(x - x_j)\, dx. \tag{A9}$$

The first term in the right member of Eq. (A9) represents the kinetic energy of the system and the second term represents the electrostatic energy U. The latter term may be conveniently evaluated using the Fourier transformed array $\bar{\alpha}_n$,

$$U(t) = 2 \sum_{n=0}^{J-1} \bar{\alpha}_n \bar{\alpha}_{-n} \sin^2 \frac{\pi n}{J} \left(1 - \frac{2}{3} \sin^2 \frac{\pi n}{J}\right). \tag{A10}$$

APPENDIX B: Diffusion Rates on a Discrete Grid

After reconstruction, the distribution function is not defined on a continuum as assumed in Section 3d, but only at discrete grid points $k\Delta v$ and we have

$$\tilde{f}(v) = \sum_j f_j \sum_k w(v - v_j)\, \delta(v - k\, \Delta v).$$

Taking the Fourier transform with respect to velocity yields

$$\tilde{H}(q) = \sum_j f_j \sum_k w(k\, \Delta v - v_j)\, e^{ikq\Delta v}.$$

Let $j'\Delta v$ denote the grid point closest to the left of v_j and $p_j = v_j/\Delta v - j'$. We have

$$\tilde{H}(q) = \sum_j W_G(q, p_j)\, f_j e^{iqv_j}, \tag{B1}$$

with

$$W_G(q, p_j) = \sum_{k'=1-O}^{O} w[(k' - p_j)\, \Delta v]\, e^{i(k'-p_j)q\Delta v}. \tag{B2}$$

Comparing Eq. (B1) with Eq. (17) we observe that the function $W_G(q, p_j)$ plays the role of the smoothing function $W(q)$ introduced in Section 3d. However, since $W_G(q, p_j)$ depends on p_j, i.e., on the location of particle j relative to the

nearest grid points, it cannot be factored out of the sum as done in Eq. (17). It appears that each particle is diffused at a different rate depending on its location relative to the nearest grid points. Particles located midway between two grid points ($p_j = 1/2$) are diffused most, while for particles approaching a grid point ($p_j \to 0$ or $p_j \to 1$) the diffusion goes to zero.

If we assume that the particles are located at random between grid points with uniform probability, the diffusion rate $D_G(q, p) = 1 - W_G(q, p)$ may be averaged to give

$$\begin{aligned} \langle D_G(q) \rangle &= 1 - \int_0^1 W_G(q, p)\, dp \\ &= 1 - \sum_{k'=1-Q}^{Q} \int_0^1 w[(k' - p)\, \Delta v]\, e^{i(k'-p)q\Delta v}\, dp. \end{aligned} \tag{B3}$$

Setting $v = (k' - p)\, \Delta v$, the sum in the last equation reduces to

$$W(q) = \int_{-\infty}^{+\infty} w(v)\, e^{iqv}\, \frac{dv}{\Delta v}.$$

This expression is identical to the Fourier transform of the weight function considered in Section 3d. For linear and quadratic weight functions, we have, respectively,

$$W^{(1)}(q) = [1/(q\Delta v/2)^2] \sin^2(q\Delta v/2), \tag{B4}$$

and

$$W^{(2)}(q) = [1/(q\ \Delta v/2)^2] \sin^2(q\ \Delta v/2)\ [1 + (\sin(q\ \Delta v)/q\ \Delta v) - \cos^2(q\ \Delta v/2)]. \tag{B5}$$

These expressions yield the curves shown in Fig. 4 and the diffusion rates given in Table I.

If we assume that the particles remain close to the grid points, a different estimate of the diffusion rates may be obtained by expanding $W_G(q, p)$ for small p. For small values of q we may also expand as in Eqs. (20) and for quadratic weight functions this gives

$$D_G(q, p) \simeq -\frac{q^4 p}{4!} \left(\frac{\partial^5 W_G}{\partial q^4\, \partial p} \right)_{\substack{q=0 \\ p=0}} = 12\, \frac{\delta v}{\Delta v} \left(\frac{q\, \Delta v}{\pi} \right)^4.$$

This estimate of the diffusion rates is applicable in the x direction to small values of the velocity for which $|\, \delta x\, | \ll \Delta x$. In the velocity direction it is applicable to regions of weak electric field for which $|\, \delta v\, | \ll \Delta v$.

ACKNOWLEDGMENTS

The author would like to express his gratitude to the Plasma Simulation Groups at the Naval Research Laboratory, and at the Princeton Plasma Physics Laboratory, and particularly to Professor John M. Dawson for many informative and stimulating discussions.

REFERENCES

1. J. M. DAWSON AND R. SHANNY, *Phys. Fluids* **11** (1968), 1506.
2. C. K. BIRDSALL AND D. FUSS, *J. Computational Phys.* **3** (1969), 494.
3. R. L. MORSE AND C. W. NIELSON, *Phys. Fluids* **12** (1969), 2418.
4. J. P. BORIS AND K. V. ROBERTS, *J. Computational Phys.* **4** (1969), 552.
5. J. A. BYERS AND M. GREWAL, *Phys. Fluids* **13** (1970), 1819.
6. J. M. DAWSON, *Phys. Rev.* **118** (1960), 381.
7. G. KNORR, *Z. Naturforsch. A* **16** (1961), 1320.
8. K-W LI, Plasma Physics Group, University of Wisconsin Report PLP 360; see also K. R. Symon, Fourth Conference on Numerical Simulation of Plasmas, Washington, D. C., 1970.
9. P. H. SAKANAKA, C. K. CHU AND T. C. MARSHALL, *Phys. Fluids* **14** (1971), 611.
10. H. L. BERK AND K. V. ROBERTS, *Phys. Fluids* **10** (1967), 1595.
11. G. KNORR, *Z. Naturforsch. A* **18** (1963), 1304.
12. T. P. ARMSTRONG, *Phys. Fluids* **10** (1967), 1269; see also T. P. ARMSTRONG AND C. W. NIELSON, *Phys. Fluids* **13** (1970), 1880.
13. D. LYNDEN-BELL, *Mon. Not. R. Astr. Soc.* **136** (1967), 101.
14. H. CRAMER, "Mathematical Methods of Statistics," pp. 89–103, Princeton University Press, Princeton, NJ, 1946.
15. J. W. COOLEY AND J. W. TURKEY, *Math. Comp.* **19** (1965), 297.
16. Computer programs implementing the fast Fourier transform algorithm were contributed by Jay Boris.
17. F. C. GRANT AND M. R. FEIX, *Phys. Fluids* **10** (1967), 696.
18. J. DENAVIT AND W. L. KRUER, *Phys. Fluids* **14** (1971), 1782.
19. H. R. LEWIS, "Methods of Computational Physics," vol. 9, p. 307. Academic Press, New York, 1970.
20. M. ABRAMOWITZ AND I. A. STEGUN, "Handbook of Mathematical Functions," pp. 878–879, Dover, New York, 1965.